

The Spatial Variation of the $3\mu\text{m}$ Dust Features in Circinus

M. D. Colling^{1*}, P. F. Roche¹ and R. E. Mason²

¹*Astrophysics, Department of Physics, University of Oxford, DWB, Keble Road, Oxford OX1 3RH*

²*Gemini Observatory, Northern Operations Center, Hilo, HI 96720*

Accepted 0000 December 00. Received 0000 December 00; in original form 0000 November 00

ABSTRACT

We report spatially-resolved variations in the $3.4\text{-}\mu\text{m}$ hydrocarbon absorption feature and the $3.3\text{-}\mu\text{m}$ polycyclic aromatic hydrocarbon (PAH) emission band in the Circinus galaxy over the central few arcsec. The absorption is measured towards warm emitting dust associated with Coronal line regions to the east and west of the nucleus. There is an absorption optical depth $\tau_{3.4\mu\text{m}} \sim 0.1$ in the core which decreases to the west and increases to the east. This is consistent with increased extinction out to ~ 40 pc east of the core, supported by the Coronal emission line intensities which are significantly lower to the east than the west. PAH emission is measured to be symmetrically distributed out to ± 4 arcsec, outside the differential extinction region. The asymmetry in the $3.4\text{-}\mu\text{m}$ absorption band reflects that seen in the $9.7\text{-}\mu\text{m}$ silicate absorption band reported by Roche et al. (2006) and the ratio of the two absorption depths remains approximately constant across the central regions, with $\tau_{3.4\mu\text{m}}/\tau_{9.7\mu\text{m}} \sim 0.06 \pm 0.01$. This indicates well-mixed hydrocarbon and silicate dust populations, with no evidence for significant changes near the nucleus.

Key words: galaxies: individual: Circinus - galaxies: ISM - galaxies: nuclei - infrared: nuclei - dust

1 INTRODUCTION

The Circinus galaxy is the nearest Active Galactic Nucleus (AGN) to the Milky Way at ~ 4 Mpc distance. The galaxy is a SAB spiral inclined at about 65° , suffering Galactic extinction of $A_v \sim 1.7$ mag (Freeman et al. 1977; Jones et al. 1999). The nucleus is a Seyfert 2, with high-excitation emission lines and an obscured broad line emission region revealed by polarimetry (Oliva, Marconi & Moorwood 1999). A strong ionization cone is detected in the optical, particularly well defined by HST [O III] filter imaging in Wilson et al. (2000). A star formation ring is identified about the Circinus galaxy nucleus at a radius of ~ 10 arcsec from H_α and [S II] imaging (Marconi et al. 1994).

Because of the proximity of the Circinus galaxy, hereafter Circinus, spectroscopy at high spatial resolution can be undertaken, with 1 arcsec corresponding to ~ 20 pc. Observations of Circinus in the mid-infra-red (MIR) at $10\ \mu\text{m}$ have showed spatial variations in the silicate-dust absorption spectra within ± 2 arcsec from the nucleus. The variation is asymmetric and consistent with there being an extended dusty torus-like structure of diameter ~ 80 pc around the Seyfert 2 core, inclined at an angle similar to the disc of the galaxy (Roche et al. 2006). Interferometric observations in the MIR by Tristram et al. (2007) are well fit with a clumpy

torus model for a cool dust component extending out to 1-pc, half-light radius. Whether these components are part of a continuous structure, and whether they are further linked to a water maser disc of diameter 0.2-0.8 pc around the core, aligned with the inner and outer dust structures and nearly orthogonal to the ionization cone (Greenhill et al. 2003), is unknown.

Studies of the $3.4\text{-}\mu\text{m}$ hydrocarbon absorption in the Milky Way have shown that it arises from the diffuse interstellar medium (ISM) (e.g. Pendleton et al. 1994; Chiar et al. 2002), the optical depth varying greatly with position and closely correlated with the visual extinction. The absorption is deepest toward the Galactic centre and weaker toward stellar regions, suggesting that the aliphatic hydrocarbons responsible are not uniformly distributed in the Galaxy, but concentrated toward the centre (Sandford, Pendleton & Allamandola 1995). The thermal background due to sky emission in the L -band makes spatially-resolved observations of the absorption feature difficult to make from the ground, as the flux and hence the signal-to-noise ratio decreases greatly off the core. A VLT/NACO image of Circinus in the L -band shows a very compact nucleus, of 1-2 arcsec diameter, with a core FWHM of 0.185 arcsec (Prieto et al. 2004), meaning that high spatial resolution and relatively long integration times are required to investigate any spatial structure.

Polycyclic Aromatic Hydrocarbons (PAHs) are

* E-mail: mdc@astro.ox.ac.uk

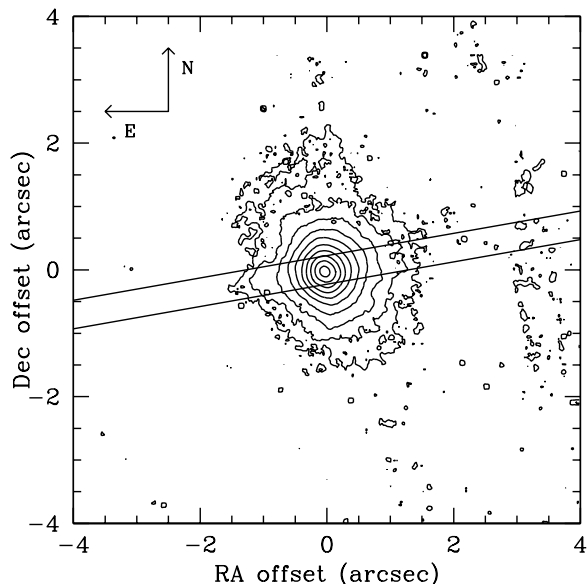


Figure 1. The GNIRS slit superimposed on the NACO L -band image of the Circinus nucleus, taken from the ESO Science Archive Facility and previously published in Prieto et al. (2004). The image is centred at the L -band emission peak, which is assumed to coincide with the active nucleus. The contours are logarithmic and separated by a factor of $\log(2)$.

identified as the emitting molecules of distinctive infra-red bands beyond $3\text{-}\mu\text{m}$ (Leger & Puget 1984; Allamandola, Tielens & Barker 1985). PAHs represent the smallest grain sizes of the dust population, excited by the far-UV (Sellgren 1984; *see review in Tielens 2008*) and destroyed by hard-UV fluxes (Aitken & Roche 1985; Leach, Eland & Price 1989). PAH emission bands were observed to be prominent in the large aperture (14×20 arcsec) ISO spectra of Circinus (Moorwood et al. 1996), but absent in a small aperture (4.2 arcsec diameter), where the flux is dominated by the nuclear emission (Roche et al. 1991). Observations of the $11.3\text{-}\mu\text{m}$ band in Circinus revealed PAH emission to be unaffected by the differential extinction detected in the nucleus, and to have a very different spatial distribution from the MIR dust continuum emission (Roche et al. 2006). Though PAH band ratios can vary, the 3.3 and $11.3\text{ }\mu\text{m}$ features are expected to have similar spatial distributions as both are thought to arise from neutral PAH emission (Allamandola et al. 1999).

The primary object of this study is to present long-slit spectroscopic observations of the $3.4\text{-}\mu\text{m}$ hydrocarbon dust absorption feature and the $3.3\text{-}\mu\text{m}$ emission band, and compare their spatial distributions to those of the silicate absorption and MIR dust emission components.

2 DATA

Spectra were taken in March 2007, programme GS-2007A-Q-41, at the Gemini South telescope with the Gemini Near-Infrared Spectrograph (GNIRS) (Elias et al. 2006). The instrument configuration covered a range of $2.9\text{ - }3.9\text{ }\mu\text{m}$ with a 0.45 arcsec wide slit with $32/\text{mm}$ grating, $R = \frac{\lambda}{\Delta\lambda} = 1700$.

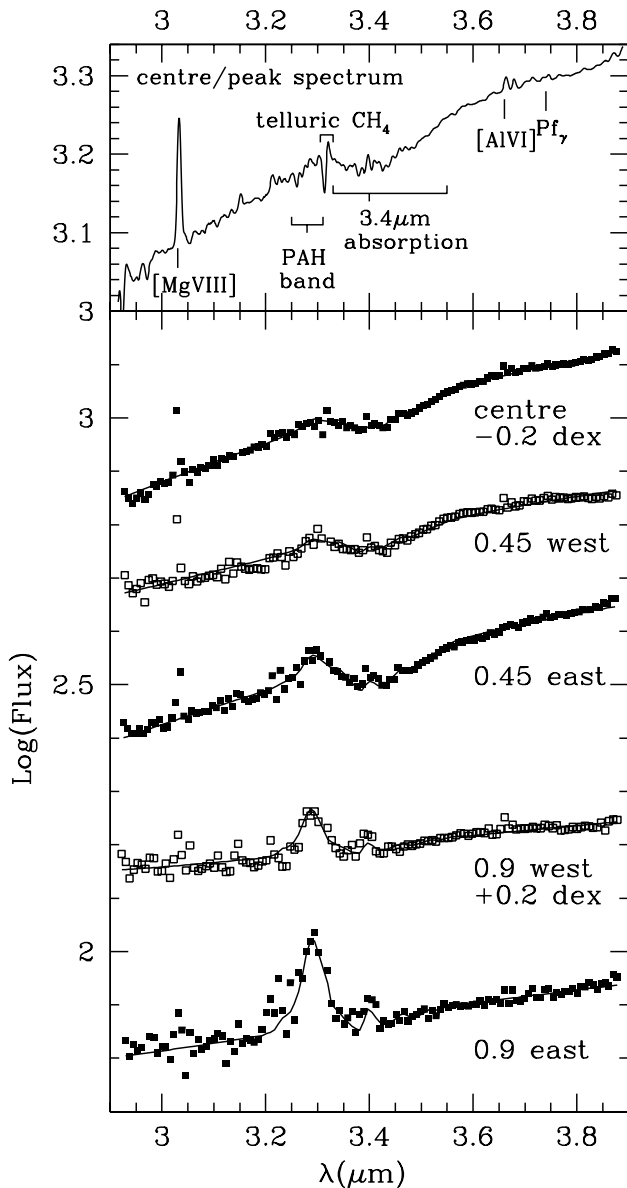


Figure 2. Five of the spectra used to measure the spatial variation of the $3\text{ - }4\text{ }\mu\text{m}$ absorption and emission. The centre spectrum together with the east and west spectra at 0.45 and 0.9 arcsec intervals. The lines are the 4-component model fits described in section 3.1. The pixels have been binned on the dispersion axis for plotting and fitting and the fluxes are offset by the values stated as appropriate. The flux is in units of $10^{-20}\text{ W cm}^{-2}\text{ }\mu\text{m}^{-1}$. The top panel shows the peak spectrum at full resolution and smoothed, with the lower panel showing the spectra after binning and smoothing.

The red sensitive, short focal length camera was used with a scale of 0.15 arcsec pixel^{-1} . The slit alignment, east/west PA 100° (see Fig. 1), was chosen to coincide with the extended emission observed in the MIR and the spatially extended spectra in that band from Roche et al. (2006).

The telescope was nodded along the slit in 10 arcsec steps. This means that the extracted spectra are effectively

differential measurements compared to reference positions 10 arcsec from the nucleus. However, here we investigate the circumnuclear emission on scales < 5 arcsec from the core, and so the effects of emission in the reference nod positions are small. The total integration time for Circinus was ~ 48 min, while for the telluric standard star, HIP 69972, it was ~ 8 min. The FWHM of the PSF is estimated to be 0.5 arcsec, at $3.79\text{-}\mu\text{m}$, from the observation of the comparison star.

The reduction was undertaken with IRAF v2.12.2a and Gemini IRAF v1.9 using the GNIRS reduction package (Cooke & Rodgers 2005). The spectra were flat-fielded, the frames coadded and a wavelength calibration applied based on the sky-emission lines that are prominent in the near-IR region. There was some evidence of detector crosstalk and a systematic, but low-level, diagonal artefact. Both of these were partially corrected for by subtracting backgrounds, composed of an average of unexposed regions, from every line of the exposed regions of the spectra. One dimensional extractions of the spectra were then produced. These were telluric-corrected and flux-calibrated, using the extracted spectrum of the standard, individually to minimise noise. The 1D spectra were binned in 0.45 arcsec intervals, comparable to the FWHM and to increase signal.

Continuum fits to the spatially-binned spectra were performed using Legendre polynomials, of order 2 or 3 dependent on the curve of the fitted spectrum. The continuum regions fit were the clear regions at 29600:29980, 31680:31860, 35940:36200, 38230:38420 \AA with particular care taken to ensure a reasonable fit across the $3.17 - 3.6 \mu\text{m}$ region. Line fluxes were found by fitting Gaussians to the lines and integrating the flux. The PAH flux and $3.4\text{-}\mu\text{m}$ feature optical depth were found using the continuum fits, from which it was decided to separate those components from the continuum flux using model fits to the spectra, described in section 3.1. Examples of the final spectra, displayed with the model fits described below, are shown in Fig. 2.

3 RESULTS

The extracted spectra show clearly the $3.4\text{-}\mu\text{m}$ absorption, the $3.3\text{-}\mu\text{m}$ emission and several spectral emission lines on top of the continuum. The compact nature of the core in Circinus is evident, as expected from the Prieto et al. (2004) imaging. Fig. 3 shows the emission is a combination of a compact nuclear component together with a more extended component attributed to diffuse galactic emission. The diffuse emission starts to dominate beyond ± 2 arcsec as seen by the change in gradient at these positions.

Model fits to the spatially-extracted, binned spectra have been used to find the absolute and relative values of the primary components in the spectra. Section 3.1 describes the model and the following sections analyse the $3.4\text{-}\mu\text{m}$ feature and the PAH emission. The spectra were analysed from the peak flux outwards, with the eastward and westward sides being compared to look for evidence of asymmetry. Spatially-extended emission from hydrogen and forbidden emission lines have also been measured and analysed and this is reported in the final section.

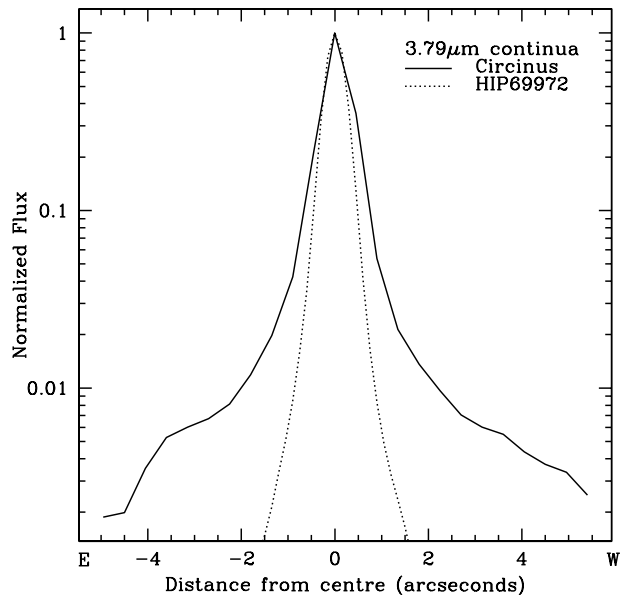


Figure 3. The normalized spatial profiles of the continuum at $3.79\text{-}\mu\text{m}$ in Circinus and the reference star.

3.1 Model fits

A model consisting of four components has been fitted to the data. A warm blackbody with $T=540$ K represents the dust emission from the inner core. The $3.4\text{-}\mu\text{m}$ absorption feature was applied to this component. The spectral profile used was that of the spectrum of IRS-6E in the Galactic centre (GC) from Pendleton et al. (1994). This shows the $3.4\text{-}\mu\text{m}$ hydrocarbon feature with well-defined double peaks in the optical depth at 3.38 and $3.42 \mu\text{m}$. A second profile, from Adamson et al. (2003) of the GC was also tested. This shows an extended bimodal absorption profile from 3.2 to $3.6 \mu\text{m}$, with features from the $3.4\text{-}\mu\text{m}$ aliphatic hydrocarbon band described above and a broader $3.3\text{-}\mu\text{m}$ absorption, attributed to PAHs. However, this introduced a degeneracy between the absorption and PAH emission that cannot be resolved. The IRS-6E profile was used to produce the final fits.

The other two components were the PAH emission complex at $3.2 - 3.6 \mu\text{m}$, obtained from the spectrum of planetary nebula NGC 7027 (Roche et al. 1996), and a hot blackbody component, fixed at 1800 K. The PAH component includes the prominent peak at $3.28\text{-}\mu\text{m}$ and the weaker peaks and plateau emission between 3.4 and $3.6 \mu\text{m}$. The profile was extracted by fitting a linear continuum to the flux at 3.1 and $3.7\text{-}\mu\text{m}$, and provides an adequate match to the PAH emission in Circinus. The hot component represents diffuse galactic emission from stellar photospheres, hot dust emission from circumstellar shells and the diffuse dust continuum, which together combine to give an effective temperature of ~ 1800 K in this spectral region. It is expected to become increasingly important in the spectra further from the core, as the diffuse galaxy starlight and dust emission begins to dominate the continuum. Initially the temperatures of the two blackbodies were allowed to float and were found to roughly converge on the temperatures above. These were

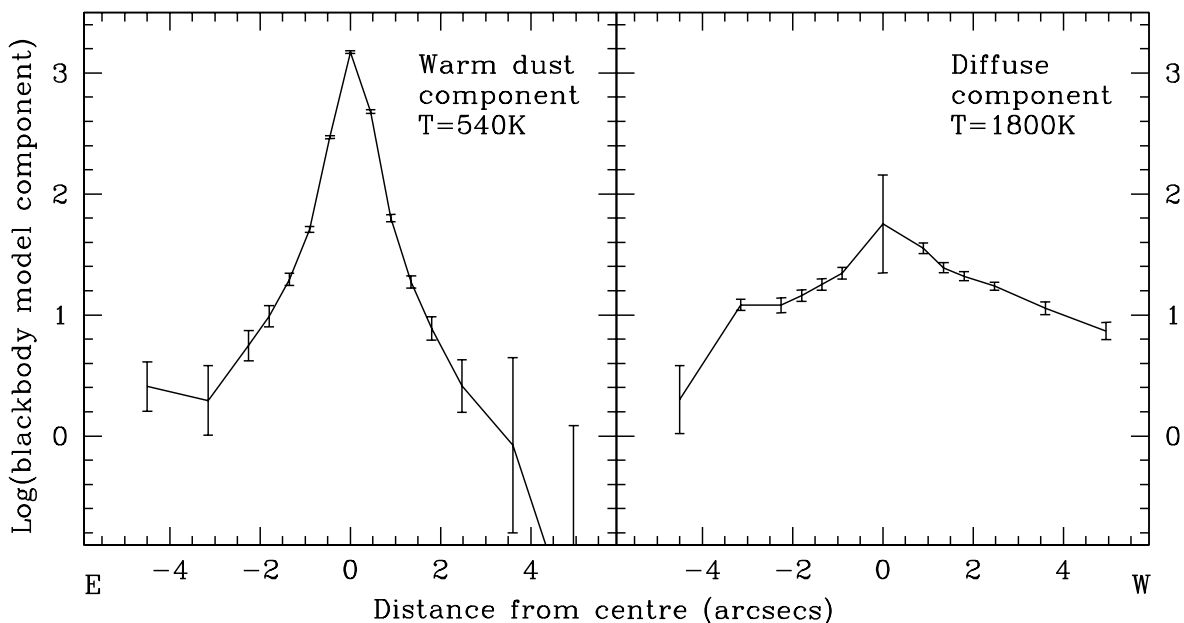


Figure 4. The spatial distributions of the continuum components from the model fits, described in section 3.1. The warm dust component is fixed at 540 K and represents the dust emission from the core. The hot component is fixed at 1800 K and represents diffuse photospheric and dust emission from stars in the host galaxy. The warm dust component is found to peak centrally very strongly and then decrease rapidly further from the core. The stellar component is also peaked centrally, but is proportionally weaker, and decreases more slowly with distance from the core. The combination of these two components reflects the shape of the continuum dust emission observed at $3.79\text{-}\mu\text{m}$ in Fig. 3.

then fixed to decrease any degeneracy of components when converging the fits with the PAH and $3.4\text{-}\mu\text{m}$ components. The models were applied using a chi-squared convergence algorithm, to find the best fit to the data for the relative strengths of the four components.

Fig. 4 shows the contributions to the continuum from the warm dust population and the diffuse hot component. Both populations are symmetric and centrally peaked, with the warm dust contributing an order of magnitude more flux on the nucleus. The diffuse emission proportion increases with distance from the core. At the central position, the contribution from the diffuse $T=1800\text{ K}$ component is small compared to the warm component and the uncertainties very large. This distribution justifies the application of the absorption profile to only the warm dust component in the model. The separation of the stellar emission from the absorption also has the benefit of removing any quenching of the absorption feature as suggested in Imanishi (2000).

3.2 $3.4\text{-}\mu\text{m}$ hydrocarbon absorption

Taking the peak flux to be coincident with the core, the core spectrum shows clear evidence of the $3.4\text{-}\mu\text{m}$ aliphatic hydrocarbon absorption. There the optical depth of the absorption is $\tau_{3.4\mu\text{m}} = 0.109 \pm 0.004$. This corresponds to $A_v = 15\text{-}25$ mag using the Galactic dust extinction relation (Pendleton et al. 1994). This is comparable to the minimum 30 mag extinction derived from the silicate absorption

(Roche et al. 2006). The right-hand figure of Fig. 5 shows how the optical depth varies with spatial position from the centre. The absorption rises to the east of the core, peaking at $\sim 0.5\text{ - }0.9$ arcsec, before decreasing beyond that. The absorption to the west appears to decrease with distance from the core and is undetected beyond 1 arcsec. These detection limits are due to both the decreasing absorption optical depth and the decreasing continuum contribution from the warm dust component against which the absorption can be detected, while the relative contribution from the diffuse hot component increases. The resulting spatial profile is consistent with there being a thick disc/torus shaped structure inclined at an angle similar to that of the galaxy. A structure of this type is also consistent with the silicate dust distribution, as suggested in Roche et al. (2006).

Table 1 shows the spatial variation of the $\tau_{3.4\mu\text{m}}/\tau_{9.7\mu\text{m}}$ ratio, with the peak value at $\tau_{3.4\mu\text{m}}/\tau_{9.7\mu\text{m}} = 0.055$. This is close to the Milky Way GC diffuse ISM ratio, which is 0.05-0.06 (using $\tau_{3.4\mu\text{m}} \sim 0.2$ from Pendleton et al. (1994) and $\tau_{9.7\mu\text{m}} \sim 3.6$ from Roche & Aitken (1985)). The Circinus ratio is also a relatively low value compared to observations of other nearby galaxies. Imanishi (2000) showed that the ratio of the absorption depths is spread from 0.02-0.23 between galaxies in his sample, with galaxies viewed at higher inclinations exhibiting lower ratios than those viewed face-on. Circinus is consistent with this finding, being at an inclination of 65° (Freeman et al. 1977).

Whilst the optical depths of the silicate and $3.4\text{-}\mu\text{m}$ ab-

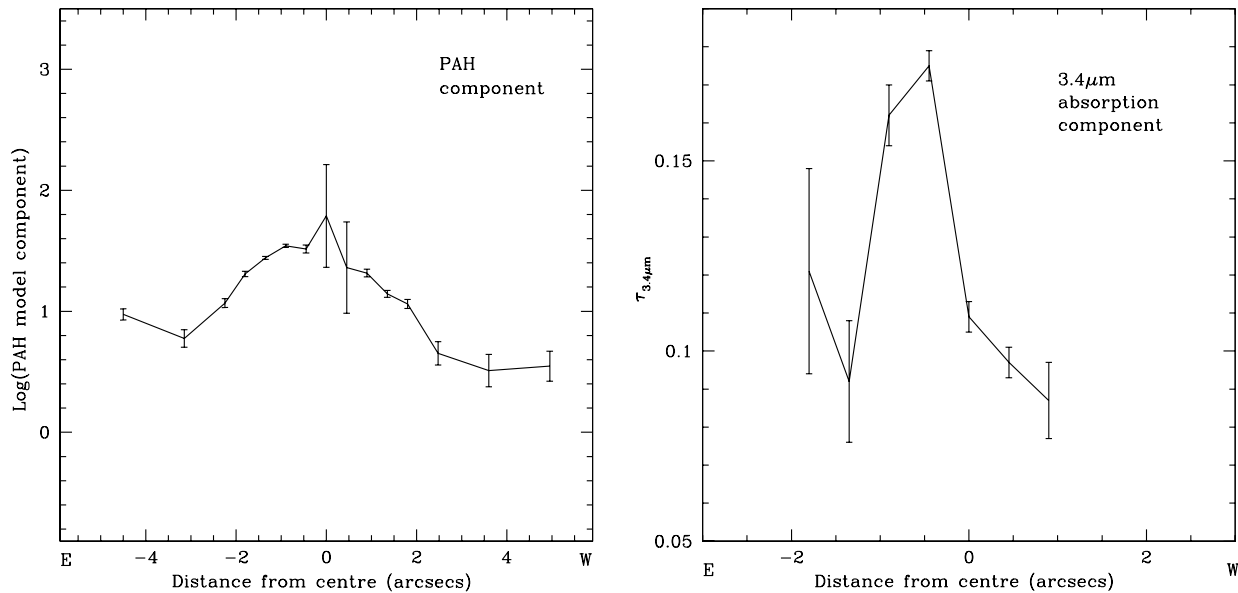


Figure 5. The spatial variation of the $3.3\text{-}\mu\text{m}$ PAH emission flux (left) and the $3.4\text{-}\mu\text{m}$ hydrocarbon absorption (right) from the model fits. Errors are estimates from the model fitting process and do not fully reflect any systematic effects in the data. The PAH emission measured in the very centre is a small component against a large continuum and the uncertainties reflect this. Note that the spatial scale is smaller for the right-hand plot than in previous plots because the $3.4\text{-}\mu\text{m}$ absorption is undetected beyond 2 arcsec to the east and 1 arcsec to the west (see text).

Distance from centre (arcsec)	$\tau_{3.4\mu\text{m}}$	$\tau_{9.7\mu\text{m}}$	$\tau_{3.4\mu\text{m}} / \tau_{9.7\mu\text{m}}$
-1.80 (E)	0.121	2.16	0.056 ± 0.0140
-1.35	0.092	2.64	0.035 ± 0.0066
-0.90	0.162	2.45	0.066 ± 0.0063
-0.45	0.175	2.04	0.086 ± 0.0087
0.0	0.109	1.98	0.055 ± 0.0059
0.45	0.097	1.91	0.051 ± 0.0057
0.90 (W)	0.087	1.28	0.068 ± 0.0130

Table 1. The spatial variation of the $\tau_{3.4\mu\text{m}}/\tau_{9.7\mu\text{m}}$ ratio in Circinus. $\tau_{9.7\mu\text{m}}$ values interpolated from Roche et al. (2006)

sorptions change by a factor of 2, the $\tau_{3.4\mu\text{m}}/\tau_{9.7\mu\text{m}}$ ratio remains approximately constant over a spatial scale of $\sim 60\text{pc}$. This indicates that the aliphatic hydrocarbons and silicates are in one well-mixed dust population, with no evidence for any variation near the Seyfert nucleus.

3.3 $3.3\mu\text{m}$ PAH emission

The PAH component from the model fits (Fig. 5) shows an emission plateau or gentle decline away from the nucleus, almost symmetric on each side. The strong continuum emission at the nucleus precludes a definitive detection of the $3.3\text{-}\mu\text{m}$ emission band in the core. Its spatial dependence is similar to that of the hot blackbody component, suggesting that diffuse hot dust may contribute to both the continuum and the PAH emission. The profile is broadly similar to the $11.3\text{-}\mu\text{m}$ PAH emission, in both east/west and north/south alignments, from Roche et al. (2006), and

very different from the distributions of the nuclear warm dust component. This clearly suggests a geometry different to the inner dust populations. The PAH emission region is not affected by the differential extinction of the aliphatic hydrocarbons and we conclude that it is therefore outside the primary absorption feature region. The finding corroborates that found in Circinus at $11.3\text{-}\mu\text{m}$ (Roche et al. 2006) and is consistent with the destruction of PAHs in high excitation regions (Aitken & Roche 1985). The spatial emission profile suggests that the PAH emission is excited primarily by diffuse emission.

3.4 Line emission

Line emission is detected to about two arcsec on each side of the nucleus, detections at the extremes partly dependent on the intrinsic flux of the line. Five lines have been firmly identified; two forbidden lines, [Mg VIII] at $3.03\text{-}\mu\text{m}$ and [Al VI] at $3.66\text{-}\mu\text{m}$, and three hydrogen Pfund-series lines, H I 10-5 (Pf_ϵ) at $3.04\text{-}\mu\text{m}$, H I 9-5 (Pf_δ) at $3.30\text{-}\mu\text{m}$ and H I 8-5 (Pf_γ) at $3.74\text{-}\mu\text{m}$. The [Al VIII] line at $3.70\text{-}\mu\text{m}$ may also be present, but is coincident with a Ca I absorption in the standard star and thus cannot be measured reliably. The spatially-extended emission of the most prominent lines is shown in Fig. 6.

Roche et al. (2006) show that the emission from the $12.81\text{-}\mu\text{m}$ [Ne II] line and the $10.52\text{-}\mu\text{m}$ [S IV] line is slightly stronger to the west of the centre than the east. The [Si VI] ($1.96\text{-}\mu\text{m}$) and [Al IX] ($2.04\text{-}\mu\text{m}$) lines have also been imaged by Maiolino et al. (1998) and show spatially-extended emission, which in their fig. 4 shows greater emission to the west of the continuum peak. Similarly from this work, the for-

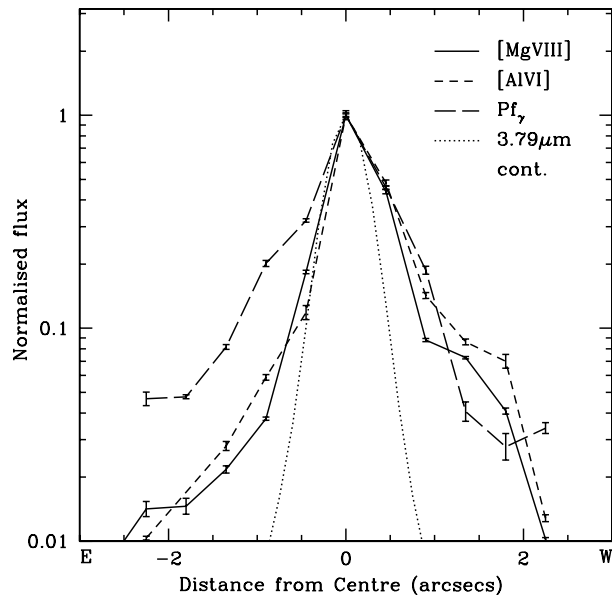


Figure 6. Integrated fluxes of 3 emission lines and the PSF/continuum from the stellar calibrator. The fluxes have been normalized to allow comparison of the spatial profiles of the lines. The high-excitation forbidden lines are asymmetric, suggesting increased extinction to the east as discussed in the text. The H I 8-5 line (Pf_γ) has a symmetrical profile yet is centrally peaked suggesting that the H II emission arises from a more diffuse component.

bidden lines $[\text{Mg VIII}]$ and $[\text{Al VI}]$ show higher intensities to the west. This is interpreted as a result of increased extinction to the east, probably due to an extended dusty disk-like structure obscuring underlying symmetric emission regions. The flux ratios of the $[\text{Mg VIII}]$, $[\text{Al VI}]$, $[\text{S IV}]$ and $[\text{Ne II}]$ lines on the east and west sides of the nucleus, are approximately in accord with the wavelength dependence of extinction in the IR (Lutz 1999), consistent with the suggestion that IR extinction is largely responsible for the observed east/west asymmetry.

The Pfund series H lines show a different distribution to those of the forbidden lines. The strongest detection, Pf_γ , shows a centrally-peaked but roughly symmetric spatial distribution about the nucleus. The only comparable line from the literature is the Br_γ line at $2.17\text{-}\mu\text{m}$, imaged in Circinus by Maiolino et al. (1998). This too shows a symmetric distribution about the peak with a spatially extended profile, as seen in Fig. 6. This naturally suggests that there are contributions to the Pf_γ flux from both a high excitation nuclear component and from diffuse emission largely outside the cold dust extinction region shown by the $3.4\text{-}\mu\text{m}$ absorption. Hydrogen in this region is presumably primarily ionized by flux from the circumnuclear star formation.

4 DISCUSSION

The origin of the extended $T\sim 500\text{ K}$ dust emission and extended coronal line emission presented above is not clearly understood. Emission at $\sim 100^\circ$ PA extending to the east

and west for >1 arcsec is clearly present in the $10\text{-}\mu\text{m}$ and $20\text{-}\mu\text{m}$ bands (Packham et al. 2005). A similar structure is evident in the $[\text{Si VII}]$ image from Prieto et al. (2004) while there is a suggestion of it in their M' $4.8\text{-}\mu\text{m}$ band image. This extended emission is not visible in the L -band image of Prieto et al. (2004), presumably because it is swamped by the stronger diffuse component, which is separated out in our spectra by the model fitting. The extended dust emission is coincident with the coronal line emitting region and therefore a reasonable explanation is that dust is heated by trapped line emission in the ionization cones. The emitting dust must be refractory and able to survive in this harsh environment, and provides a background source against which the $3.4\text{-}\mu\text{m}$ absorption can be measured. The symmetry of the $8.8\text{-}\mu\text{m}$ image of Packham et al. (2005) to the east and west suggests that the intrinsic L -band continuum dust emission is also symmetric across the nucleus. Variations in the emission line intensities and the $3.4\text{-}\mu\text{m}$ hydrocarbon absorption depth are then primarily due to variations in extinction due to changes in the absorbing dust column along the line of sight. An illustration of such a configuration is shown in Fig. 7.

The ratio of the hydrocarbon to silicate dust optical depths, $\tau_{3.4\mu\text{m}}/\tau_{9.7\mu\text{m}}$, is fairly constant across a projected distance of 60 pc in the nuclear region of Circinus. This compares to significant variations found between galaxies by Imanishi (2000). Imanishi suggested that a possible explanation for these variations could be that the $9.7\text{-}\mu\text{m}$ silicate dust column probes the line of sight to dust emission at $T\sim 300\text{ K}$, while the $3.4\text{-}\mu\text{m}$ hydrocarbon band probes to dust emission at $T\sim 1000\text{ K}$, and that temperature gradients in the circumnuclear dust could then produce variations in the $\tau_{3.4\mu\text{m}}/\tau_{9.7\mu\text{m}}$ ratio. While, the observations presented here are not sensitive to temperature gradients within the central 10pc, we see no evidence for temperature gradients in the dust emission beyond that and no evidence of variations in $\tau_{3.4\mu\text{m}}/\tau_{9.7\mu\text{m}}$. It seems that the paths to the $3\text{ }\mu\text{m}$ and $10\text{ }\mu\text{m}$ emitting regions in Circinus are similar, and that the hydrocarbon and silicate components of the dust are well mixed, with a ratio similar to that found towards the Galactic centre in the Milky Way. It is striking that any variations within the $\tau_{3.4\mu\text{m}}/\tau_{9.7\mu\text{m}}$ ratio in Circinus are much smaller than the variations between galaxies (Imanishi 2000).

The $3.3\text{-}\mu\text{m}$ PAH emission band has a very different and much broader spatial distribution to the continuum emission. It is similar to that of the $11.3\text{-}\mu\text{m}$ feature (Roche et al. 2006) and to the diffuse galactic emission, suggesting that it is excited primarily by a diffuse radiation field rather than the AGN, and in accord with the expectation that the carriers are destroyed by the hard photons around the nucleus (Aitken & Roche 1985).

5 CONCLUSIONS

Long slit spectra of the Circinus galaxy between 2.9 and $3.9\text{ }\mu\text{m}$ at a spatial resolution of ~ 0.5 arcsec are presented. The continuum emission from the nuclear region is separated into two components, a compact core with dust emission at $T\sim 540\text{ K}$ and a diffuse component, represented by a $T=1800\text{ K}$ blackbody. The flux from the compact core and the extended east-west structure dominates the emis-

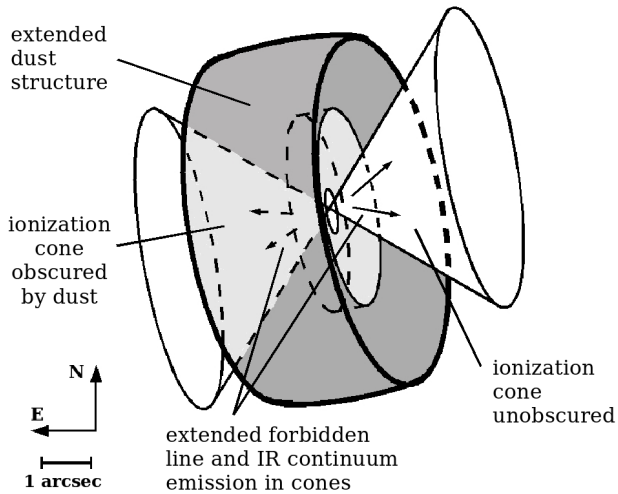


Figure 7. Sketch of the proposed extended dust structure for Circinus from 3 and $10\text{-}\mu\text{m}$ observations. The inner IR continuum emission is from dust heated by radiation from the core, while the extended east-west continuum emission is from dust heated in the ionization cones. An inclined dusty thick structure produces the differential east-west extinction (see text).

sion within the central ~ 3 arcsec. The $3.4\text{-}\mu\text{m}$ aliphatic hydrocarbon absorption has been measured towards this emission structure. The optical depth is $\tau_{3.4\mu\text{m}} \sim 0.1$ towards the nucleus, but changes by a factor of 2 in the central 60 pc, decreasing to the west but increasing to the east. Similar variations have been found in the depth of the $9.7\text{-}\mu\text{m}$ silicate absorption (Roche et al. 2006), while the asymmetry in the [Mg VII] and [Al VI] emission line intensities on either side of the nucleus also suggests significant differential extinction. All of these observations are consistent with a coronal line region containing warm emitting dust and extending east and west from the nucleus. The nucleus is obscured with $A_V \sim 25$ mag, which increases to ~ 40 mag at 1 arcsec to the east and decreases to the west. This may indicate an inclined dusty disc-like structure, with the east side inclined toward us and lying behind the coronal line region on the west side. Large scale dusty disks appear to be a common feature in the few AGN that have been probed spectroscopically at subarcsecond resolution (e.g. Mason et al. (2006), Roche et al. (2006), Young et al. (2007)), and adaptive optics correction would permit higher resolution measurements of the dust properties in the L-band.

The ratio of $\tau_{3.4\mu\text{m}}/\tau_{9.7\mu\text{m}} \sim 0.06$ for Circinus is comparable to the Galactic value (Pendleton et al. 1994). It remains approximately constant within the region for which both absorptions are detected, from ~ 40 pc east to 20 pc west (~ 90 and 50 pc projected distance on a 65° disc). This indicates that the two dust populations are well-mixed within the central region and neither is preferentially destroyed or suppressed. The PAH population, however, has a flatter spatial emission profile across the inner ± 2 arcsec, indicating PAHs are not primarily excited by the nuclear flux or are absent in the inner region. The PAH distribution more closely resembles the diffuse galactic emission and is likely to be related to the circumnuclear star-formation regions (Marconi et al. 1994).

ACKNOWLEDGMENTS

This work is based on observations obtained at the Gemini Observatory, which is operated by the Association of Universities for Research in Astronomy, Inc., under a cooperative agreement with the NSF on behalf of the Gemini partnership: the National Science Foundation (United States), the Science and Technology Facilities Council (United Kingdom), the National Research Council (Canada), CONICYT (Chile), the Australian Research Council (Australia), Ministério da Ciência e Tecnologia (Brazil) and SECYT (Argentina). This work has made use of the NASA/IPAC Extragalactic Database (NED) which is operated by the Jet Propulsion Laboratory, California Institute of Technology, under contract with the National Aeronautics and Space Administration. We thank the Gemini Observatory and particularly the staff at Gemini-S for assistance in collecting these data. M. C. thanks the U. K. Science and Technology Facilities Council for the support of a studentship. We thank the referee for helpful suggestions.

REFERENCES

- Adamson A.J. et al., 2003, AN, 324, S1, 211
 Aitken D.K., Roche P.F., 1985, MNRAS, 213, 777
 Allamandola L.J., Tielens A.G.G.M., Barker J.R., 1985, ApJ, 290, L25
 Allamandola L.J., Hudgins D.M., Sandford S.A., 1999, ApJ, 511, L115
 Chiar J.E., Adamson A.J., Pendleton Y.J., Whittet D.C.B., Caldwell D.A., Gibb E.L., 2002, ApJ, 570, 198
 Cooke A., Rodgers B., 2005, ASP Conf. Series, 347, 514
 Elias J.H., Rodgers B., Joyce R.R., Lazo M., Doppman G., Winge C., Rodríguez-Ardila A., 2006, SPIE, 6269, 36
 Freeman K.C., Karlsson B., Lynga G., Burrell J.F., van Woerden H., Goss W.M., Mebold U., 1977, A&A, 55, 445
 Greenhill L.J. et al., 2003, ApJ, 590, 162
 Imanishi M., 2000, MNRAS, 319, 331
 Jones K.L., Koribalski B.S., Elmouttie M., Haynes R.F., 1999, MNRAS, 302, 649
 Leach S., Eland J.H.D., Price S.D., 1989, J. Phys. Chem., 93, 7583
 Leger A., Puget J.L., 1984, A&A, 137, L5
 Lutz D., 1999, ESASP, 427, 623L
 Maiolino R., Krabbe A., Thatte N., Genzel R., 1998, ApJ, 493, 650
 Marconi A., Moorwood A.F.M., Origlia L., Oliva E., 1994, ESO Messenger, 78, 20
 Mason R. E., Geballe T. R., Packham C., Levenson N. A., Elitzur M., Fisher R. S., Perlman E., 2006, ApJ, 640, 612
 Moorwood A.F.M., Lutz D., Oliva E., Marconi A., Netzer H., Genzel R., Sturm E., de Graauw T., 1996, A&A, 315, L109
 Oliva E., Marconi A., Moorwood A.F.M., 1999, A&A, 342, 87
 Packham C., Radomski J.T., Roche P.F., Aitken D.K., Perlman E., Alonso-Herrero A., Colina L., Telesco C.M., 2005, ApJ, 618, L17
 Pendleton Y.J., Sandford S.A., Allamandola L.J., Tielens A.G.G.M., Sellgren K., 1994, ApJ, 437, 683
 Prieto M.A. et al., 2004, ApJ, 614, 135

- Roche P.F., Aitken D.K., 1985, MNRAS, 215, 425
Roche P.F., Aitken D.K., Smith C.H., Ward M.J., 1991, MNRAS, 248, 606
Roche P.F., Lucas P.W., Hoare M.G., Aitken D.K., Smith C.H., 1996, MNRAS, 280, 924
Roche P.F., Packham C., Telesco C.M., Radomski J.T., Alonso-Herrero A., Aitken D.K., Colina L., Perlman E., 2006, MNRAS, 367, 1689
Sandford S.A., Pendleton Y.J., Allamandola L.J., 1995, ApJ, 440, 697
Sellgren K., 1984, ApJ, 277, 623
Tielens A.G.G.M., 2008, ARA&A, 46, 289
Tristram K.R.W. et al., 2007, A&A, 474, 837
Wilson A.S., Shopbell P.L., Simpson C., Storchi-Bergmann T., Barbosa F.K.B., Ward M.J., 2000, AJ, 120, 1325
Young S., Packham C., Mason R. E., Radomski J. T., Telesco C. M., 2007. MNRAS, 378, 888